Journal of Catalysis 263 (2009) 196–204

Contents lists available at ScienceDirect

Journal of Catalysis

www.elsevier.com/locate/jcat

Grain boundary control in nanocrystalline MgO as a novel means for significantly enhancing surface basicity and catalytic activity

Roxana Vidruk [a], Miron V. Landau [a,*], Moti Herskowitz [a], Michael Talianker [b], Nahum Frage [b], Vladimir Ezersky [b], Natali Froumin [b]

[a] Blechner Center for Applied Catalysis and Process Development, Department of Chemical Engineering, Ben-Gurion University of the Negev, Beer-Sheva 84105, Israel
[b] Department of Materials Engineering, Ben-Gurion University of the Negev, Beer-Sheva 84105, Israel

ARTICLE INFO

Article history:
Received 5 January 2009
Accepted 13 February 2009
Available online 28 February 2009

Keywords:
MgO
Grain boundaries
Basicity
Catalyst

ABSTRACT

The grain boundaries in nanocrystalline MgO were formed by dehydration of densified magnesium hydroxide aerogel. Its configuration was regulated by controlling the contact interface between the nanocrystals in the hydroxide precursor. The materials with high contact interface were obtained by application of chemical (multiple aerogel condensation) and physical (pressing) densification methods. Formation of distorted zones at the grain boundaries areas in the MgO densification process increased its surface basicity by as much as 8 times at a crystal domain size of 5 nm. The grain boundaries contribution to the creation of coordinative unsaturated surface ions and vacancies in nanocrystalline MgO was determined by a variety of physical and chemical methods. The significant increase of surface basicity yielded a major enhancement of catalytic activity of densified MgO material measured in Knoevenagel condensation of benzaldehyde with malononitrile and transesterification of phenyl acetate with 1-phenylethanol.

1. Introduction

The catalytic activity of inorganic ionic crystals in many organic reactions is determined by low-coordinated surface ions (LCSI) [1]. Areas of atomic disorder formed at the interface of crystal grains — grain boundaries (GB) — were theoretically predicted to be a source of LCSI active sites in solid catalysts [2]. The stabilization of atomic disorder in these areas was confirmed further by more accurate density functional theory (DFT) calculations [3–5] and by experimental observations [3,6–9]. However, experimental implementation of LCSI in GB areas was hampered by the lack of techniques for controlled formation of GB in high-surface-area nanocrystalline ionic solids and for determination of their contribution to the LCSI content.

The current method for increasing the content of LCSI with basic functionality was to increase the dispersion of metal oxides which created LCSI at the emerging edges and corners of the metal oxide crystals [10,11]. Brønsted basic sites (surface OH groups) are formed at the surface of MgO, as a result of surface hydration [12] (Scheme 1), besides LC oxygens which are Lewis basic sites. Scheme 1 indicates that the total concentration of basic sites (both Lewis and Brønsted) is determined by the concentration of coordinative unsaturated oxygen ions at the surface of MgO crystals and their relative contribution depends on the extent of surface hydroxylation.

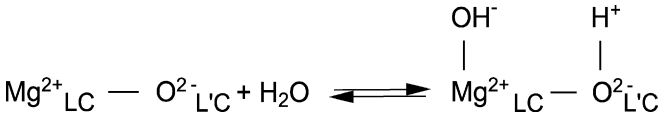

Scheme 1. Heterolytic dissociation of water at the surface of magnesium oxide (reprinted from [12]).

The efficiency of increasing the dispersion of metal oxides for creation of LCSI is limited by the confinement of LCSI to the edges, corners and kinks at the catalyst's surface and by smoothing of the crystal surface at low particle diameters that increases the coordination of the surface ions located at the edges, corners and kinks [13,14]. This study demonstrates that these limitations can be overcome by forming GB between disoriented nanocrystals of metal oxide phase. MgO nanocrystals form aggregates in which the primary crystallites are separated by very thin three-dimensional distorted zones, caused by mismatch of the atoms of one crystal with the atoms in the neighboring crystal. In the so-formed GB region, it is possible to stabilize the disordered low coordinated ions formed as a result of countercurrent atoms/ions/vacancies diffusion in crystal contacts areas. Some of crystallographical disordered ions are available on the surface of GB areas, reaching a width of up to 7 atomic

* Corresponding author. Fax: +972 (8) 6479427.
E-mail address: mlandau@bgu.ac.il (M.V. Landau).

0021-9517/$ – see front matter
doi:10.1016/j.jcat.2009.02.014

layers [15,16]. These ions can increase by an order of magnitude. The surface concentration of LCSI and vacancies play the role of catalytic active sites with basic, acidic or redox functionality. In the present work, this phenomenon was investigated using MgO as an ionic crystal with basic surface functionality, where the GB area between nanocrystal grains was controlled by densification of a magnesium hydroxide precursor or subjecting the precursor to isostatic pressure. Here we show that densification of an Mg hydroxide aerogel followed by calcination at 823 K creates high-angle or coincidence GB between disoriented MgO nanocrystals. The crystallographic disorder generated in these areas increases the surface basicity by an order of magnitude, thereby significantly enhancing the catalytic activity.

2. Experimental

2.1. Synthesis of the materials

The precursor aerogel was prepared by sol–gel processing according to Utamapanya et al. [17]. $Mg(OEt)_2$ (2 g) dissolved in anhydrous MeOH (22 ml) were added to anhydrous toluene (115 ml) and water (0.9 ml). The resulting alkoxide was hydrolyzed overnight at 298 K. The sol so obtained was transferred to an autoclave and purged with nitrogen, and the temperature was increased to 578 K at 1 $K\,min^{-1}$ to give a final pressure of 7.5 MPa. After 10 min, the pressure was decreased slowly at constant temperature. The resulting $Mg(OH)_2$ aerogel was dried in air at 393 K for 5 h.

Chemical densification of this precursor was conducted by immersing dried aerogel (1 g) into solution of $Mg(OEt)_2$ (1.3 g) in a mixture of MeOH (20 ml) and toluene (50 ml), without the addition of water. After stirring overnight at 298 K in a glove box, the liquid was removed by filtration, and the wet aerogel was placed in a glass vessel inside an autoclave. A mixture of MeOH (13 ml) and toluene (67 ml) was also placed in the autoclave next to the glass vessel. The temperature/pressure regime described above was then applied. Conducting the heating under a saturated pressure of solvents prevented drying of the aerogel. More importantly, it facilitated decomposition of the Mg-ethoxide solution at 578 K to give deposition of Mg hydroxide inside the pores of the aerogel. The procedure was repeated two more times, and samples were collected after each consecutive densification.

Physical densification of the precursor aerogel was conducted by placing the powder (10 mg) in a dye 12.6 mm diameter and applying a pressure of 1180 MPa for 1 h at 298 K.

The as-prepared aerogel and its densified products were converted to MgO by calcination in a nitrogen flow at 823 K for 2 h before characterization and catalytic testing. After calcination, the materials were handled under nitrogen or He to exclude contact with atmospheric CO_2. This measure was not taken when conducting the XRD, HRTEM, N_2-adsorption and XPS characterizations.

2.2. Characterization of the materials

Surface area, pore volume, and pore size distribution were obtained from N_2 adsorption–desorption isotherms, by using the conventional BET and BJH methods. The samples were outgassed under vacuum for 2 h at 393 K (aerogel) or 523 K (MgO). Isotherms were obtained at the temperature of liquid nitrogen with a NOVA-2000 (Quantachrome, Version 7.02) instrument.

Conventional wide-angle XRD patterns were obtained with a Philips 1050/70 powder diffractometer fitted with a graphite monochromator; software developed by Crystal Logic was used. Phase identification was performed by using BEDE ZDS computer search/match program coupled with the ICDD (International Center for Diffraction Data) Powder Diffraction File database (2006). The $Mg(OH)_2$ and MgO crystal size was determined by using the Scherrer equation $h = K\lambda/[(B^2 - \beta^2)^{0.5}\cos(2\theta/2)]$, where $K = 1.000$ is the shape factor, $\lambda = 0.154$ nm, β is the instrumental broadening correction, and B is the (002) reflection broadening at $2\theta = 42.9°$ for MgO and reflection broadening at $2\theta = 11.6°$ for magnesium hydroxide hydrate. The relative content of amorphous MgO phase represented in X-ray diffractograms by a wide reflection centered at $2\theta = 36°$ was obtained by Rietveld refinement of the XRD profile by using the DBWS-9807 program.

HRTEM analysis was conducted on a FasTEM JEOL 2010 microscope operating at 200 kV. The samples for HRTEM were prepared by depositing a drop of ethanol suspension of solid catalyst on a carbon-coated copper grid.

Titration of basic sites was conducted as follows: MgO powder (50 mg) was placed in a flask containing *o*-xylene (50 ml) with 0.1 wt% phenolphthalein indicator, under nitrogen. The suspension was stirred for 4 h at room temperature in a glove box and then titrated with a 0.05 M solution of benzoic acid in *o*-xylene. The amount of basic sites in the solid ([B], $mmol\,g^{-1}$) was calculated according to the equation: $[B] = V \times [BA]/w_{MgO}$, where V (ml) — volume of benzoic acid solution added to the suspension until the color at the solid surface disappeared completely, [BA] — concentration of benzoic acid in *o*-xylene ($mmol\,ml^{-1}$), and w_{MgO} — weight of the sample (g).

The surface basicity of the densified MgO samples was also characterized by TPD of CO_2. The experiments were performed in AMI-100 Catalyst Characterization System (Zeton-Altamira), equipped with a mass-spectrometer (Ametek 1000) for identification of components in the outlet gas. MgO (0.2 g) (after aerogel decomposition at 823 K and cooling in He flow), was saturated with 5 vol% CO_2/He at 303 K, purged with He to remove physically adsorbed CO_2 and heated in He flow at 10 $K\,min^{-1}$. The integral intensity of the TPD peaks corresponding to mass 44 (CO_2) indicated the amount of basic sites, while the positions of desorption peaks indicated the basic strength.

The nature of CO_2 moieties chemisorbed at the surface of MgO materials was determined by infrared spectroscopy (FTIR). The infrared spectra were recorded with a Nicolet Impact 460 FTIR spectrometer, with the use of KBr pellets (0.005 g sample and 0.095 g KBr), with 32 sample scans. The data were treated with OMNIC software. Spectra were taken at room temperature. Before the analysis, the samples were calcined at 823 K for 2 h in N_2, cooled to room temperature and exposed to 5% CO_2/He for 2 h. Weakly adsorbed CO_2 was removed by flushing with N_2 for about 15 min.

XPS spectra were measured with ESCALAB 250 ultra-high-vacuum (10^{-9} Torr) apparatus with Al$K\alpha$ X-ray source and monochromator. Powder samples of the catalysts were pressed on the indium-plated grid to a thin layer. The spectral components of O, Mg and C signals were found by fitting a sum of single-component lines to the experimental data by means of nonlinear least-squares curve-fitting. The single-component lines were assumed to have the shape of the sum of Cauchy and Gaussian curves, and deconvolution was performed. To correct for charging effects, all spectra were calibrated relative to a carbon 1s peak positioned at 285.0 eV.

2.3. Catalytic performance

The catalytic activity of the MgO materials was tested in two organic reactions: Knoevenagel condensation of benzaldehyde with malononitrile (RI, Scheme 2a) and transesterification of phenyl acetate with 1-phenylethanol (RII, Scheme 2b). The reactions were carried out under a nitrogen flow in a stirred glass reactor equipped with a reflux column. Toluene was used as the solvent. The catalysts were activated at 823 K under nitrogen flow

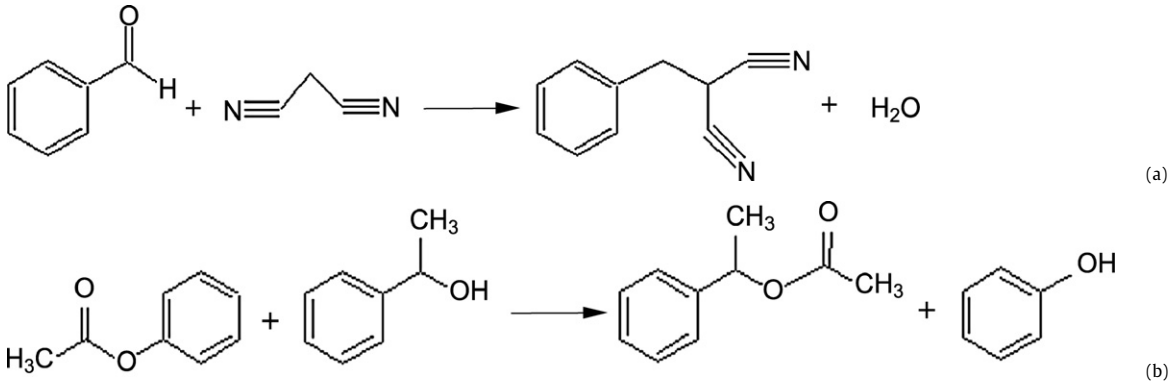

Scheme 2. Base-catalyzed reactions used for activity testing.

for 2 h before the experiment and were then transferred to the reactor under inert atmosphere to avoid exposure to air. The activated catalyst powder with the particle size in range 30–70 μm (50 mg for RI and 500 mg for RII) was added to a reaction vessel containing a mixture of 10 mmol of each reactant and 10 cm^3 of solvent heated to the reaction temperature: 313 K for RI and 383 K for RII. The intrinsic catalysts activity was estimated in a single point test conducting the reactions for periods of time needed in order to achieve 25% conversion. It was established that decreasing of the particle size and stirring did not affect the reactants conversion reflecting the absence of diffusion limitations.

Analysis of the reactions products was conducted with an Agilent 4890D GC equipped with the flame ionization detector (FID), employing a capillary column of 30 m length (HP-1) and helium as a carrier gas. The reaction rates normalized per catalyst weight and per catalyst surface unit were calculated on the basis of the amounts of products N_{prod} (mmol) (benzylidenemalononitrile in RI; α-methylbenzylacetate in RII): $\text{Rate}_W[\frac{\text{mmol}}{g\times h}] = \frac{N_{\text{prod.}}}{w_{\text{MgO}}\times t}$, $\text{Rate}_S[\frac{\text{mmol}}{m^2\times h}] = \frac{N_{\text{prod.}}}{w_{\text{MgO}}\times t\times \text{S.A.}}$, where t — reaction time (h), w_{MgO} — weight of loaded catalyst (g) and S.A. BET surface area ($m^2\,g^{-1}$) of catalyst calculated on the basis of N_2 adsorption data. The TOFs were calculated as amounts of products $N_{\text{prod.}}$ (mmol) obtained per one basic site (mmol) in a certain period of time: $\text{TOF}[\frac{\text{mmol}}{\text{mmol}_{\text{site}}\times h}] = \frac{N_{\text{prod.}}}{[\text{B}]\times w_{\text{MgO}}\times t}$, where [B] — is the concentration of basic sites ($\text{mmol}\,g^{-1}$) and t — time (h) needed for production of N_{prod} at 25% conversion.

3. Results and discussion

3.1. Effect of densification of magnesia aerogel precursor on the surface basicity of nanostructured MgO material

The GB area in the final MgO material obtained by dehydration of a magnesium hydroxide aerogel [$Mg(OH)_2{\cdot}xH_2O \rightarrow MgO + H_2O$] was regulated by controlling the contact interface between the nanocrystals in the hydroxide precursor. The materials with high contact interface were obtained by application of the two materials densification strategies. The mesopores of the starting aerogel were first filled with $Mg(OH)_2$ hydrate nanoparticles ("chemical" densification) or the aerogel material was subjected to isostatic pressure ("physical" densification) and thereafter calcined at 823 K.

The starting mesoporous aerogel, prepared by sol–gel processing, displayed surface area of 900 $m^2\,g^{-1}$ (BET), pore volume 1.98 $cm^3\,g^{-1}$ (N_2-adsorption, BJH). Its XRD patterns shown in Fig. 1a were similar to that recorded for magnesia aerogel in [17]. No crystalline Mg-hydroxide phase was found in ICDD data corresponding to these patterns. They represented a good fit to the XRD patterns of nickel hydroxide hydrate $3Ni(OH)_2{\cdot}2H_2O$ (ICCD Card # 22-4440) containing reflections at $2\theta = 11.6°$, 23.8°, 59.6° and superposition of peaks at $2\theta = 33.7$–35.2. The peaks corresponded to the planes (001), (002), (300) and (110)–(111) with d-spacings of 7.60, 3.74, 1.55 and 2.66–2.55 Å in diffractogram of $3Ni(OH)_2{\cdot}2H_2O$ phase with matching relative intensities. Based on these data it can be assumed that the parent magnesia aerogel represented a crystalline hydroxide-hydrate with triagonal symmetry (P31m, #162). Its average crystal domain size was 4 nm. Dehydration of this parent aerogel at 823 K yielded material with XRD patterns corresponding to pure MgO periclase phase with cubic structure according to ICDD Card # 43-1022 (Fig. 1b). They contained all the reflections characteristic for this phase: peaks at $2\theta = 36.0°$, 42.9°, 62.3°, 74.7° and 78.6°, corresponding to planes (111), (200), (220), (310) and (222) with d-spacings 2.43, 2.10, 1.49, 1.27 and 1.22 Å, respectively, and matching the relative intensities. The average crystal size of this material was 5 nm. It displayed surface area of 257 $m^2\,g^{-1}$, pore volume of 1.33 $cm^3\,g^{-1}$ and mean pore diameter of 10 nm corresponding to the maximum of the pore size distribution derived by BJH method from the N_2-desorption isotherm.

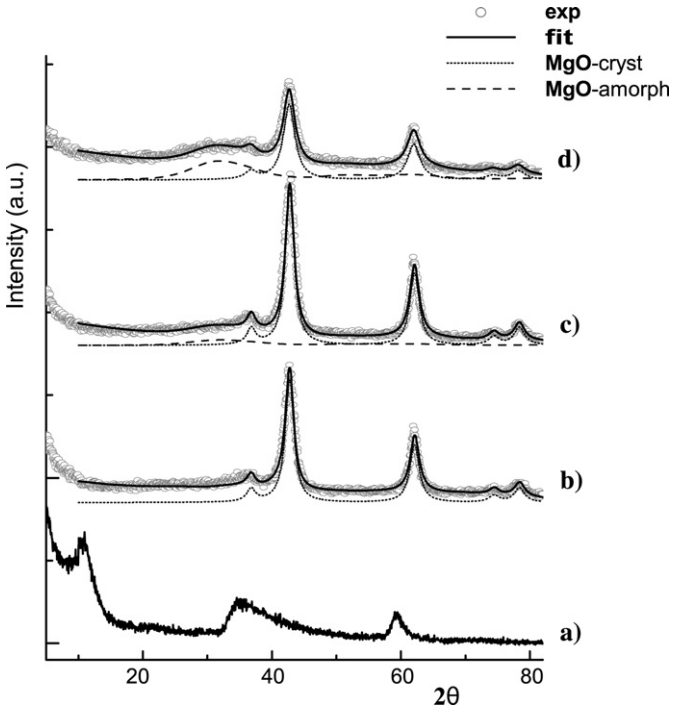

Fig. 1. X-ray diffraction patterns of: (a) starting Mg-aerogel; (b) MgO obtained after calcination of starting Mg-aerogel at 823 K; (c) MgO obtained after one chemical densification of Mg-aerogel and calcination at 823 K; (d) MgO obtained after two chemical densifications of Mg-aerogel and calcination at 823 K.

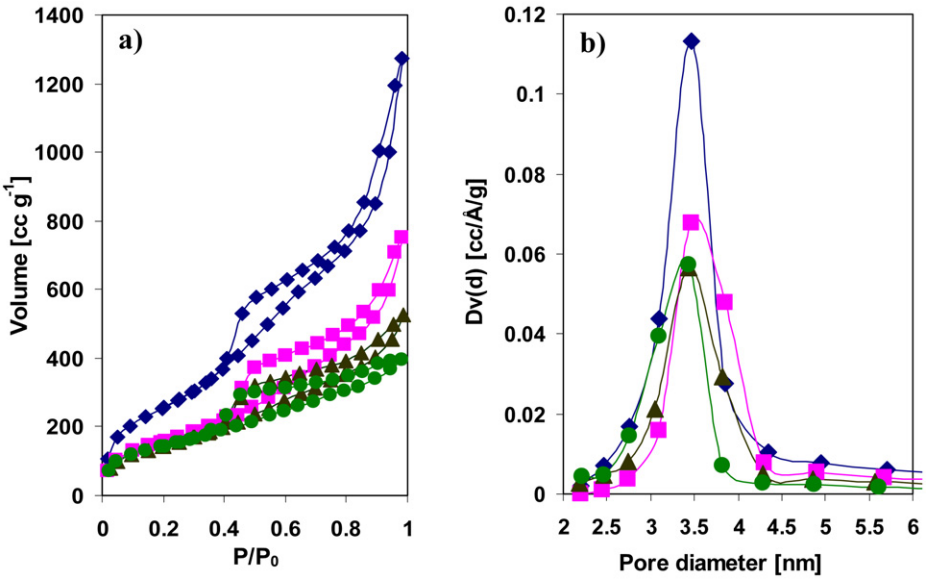

Fig. 2. Nitrogen adsorption isotherms (a) and pore size distributions (b) of the magnesium hydroxide hydrate precursors of MgO materials: (◆) starting Mg-aerogel; (■) Mg-aerogel after one chemical densification; (▲) Mg-aerogel after two chemical densifications; (●) Mg-aerogel after three chemical densifications.

Chemical densification of the starting aerogel by magnesium hydroxide deposition in one, two or three cycles caused a gradual decrease in the pore volume of the mesoporous skeleton. The N_2-adsorption–desorption isotherms and pore size distributions in parent and densified Mg-aerogel are presented in Fig. 2. The isotherms and hysteresis loops recorded with parent and densified magnesia aerogel were of type IV and H_3, respectively, according to IUPAC classification (Fig. 2a). They are characteristic of mesoporous solids built by aggregates of platy particles. The pore size distributions of parent and densified aerogel demonstrated a gradual decrease of pore volume with increasing of the number of densification steps leaving the mean pore diameter about the same 3.5–4 nm (Fig. 2b). The values of the pore volume for dried (but not calcined) material decreased from 1.98 to 1.16, 0.85, and 0.63 $cm^3\,g^{-1}$ for one, two, and three consecutive chemical densifications, respectively, thus indicating the filling of pores with magnesia. XRD patterns of these densified materials were the same meaning that the pores of the starting aerogel were filled with a magnesium hydroxide hydrate phase identical in structure and particle size to the starting material. The similar pore diameters in parent and densified Mg-aerogels assume complete blocking of the part of pores with nanoparticles of the guest Mg-hydroxide-hydrate phase which size (4 nm) is consistent with this pore diameter. It was suggested that this would serve to increase the contact interface between the nanocrystals in the $Mg(OH)_2$-hydrate precursor as well as in final MgO material obtained after decomposition of the precursors.

Calcination of aerogel at 823 K after one and two chemical densifications yielded pure MgO materials with a periclase cubic structure (Fig. 1, ICDD powder diffraction file # 4-829) and average crystal size of 5 nm. Similar pore diameters (10 nm) and crystal sizes (5 nm) were measured in MgO produced from the starting aerogel material. In the MgO produced from triply densified aerogel material, the crystal size increased to 7.5 nm. Physical densification yielded a material with crystal size 5.5 nm and surface area 181 $m^2\,g^{-1}$.

The contact interface between the MgO nanocrystals was characterized by their aggregation ratio Ψ as proposed by Royer, Duprez and Kaliaguine [9]:

$$\Psi = \mathrm{S.A.}_{\mathrm{theor}}/\mathrm{S.A.}_{\mathrm{BET}};\quad \mathrm{S.A.}_{\mathrm{theor}} = 6000/\rho_{\mathrm{MgO}} \times D,$$

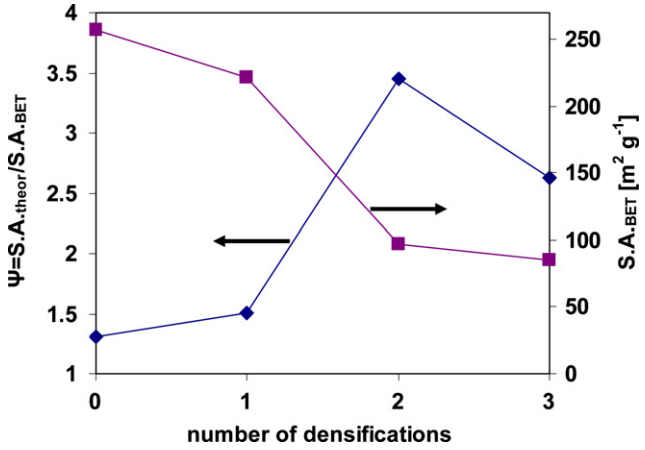

Fig. 3. Effect of chemical densification of Mg-aerogel precursor on the surface area and aggregation ratio of nanocrystals in MgO materials obtained after calcination at 823 K.

where D is MgO crystal size (nm) and ρ_{MgO} (3.585 $g\,cm^{-3}$) is the theoretical density of MgO with periclase structure derived from XRD data. The published method for calculation of $\mathrm{S.A.}_{\mathrm{theor}}$ assumed globular or cubic form of MgO nanocrystals [18]. The cubic form of nanocrystals in all MgO materials was confirmed by TEM.

The crystal aggregation ratio Ψ of the MgO obtained from the parent aerogel precursor was 1.3. Its value reached a maximum of 3.5 at two densifications and then decreased to 2.6 after triple densification of MgO precursor (Fig. 3). However, the surface area steadily decreased with the number of densifications (Fig. 3). The increase of aggregation ratio after one and two chemical densifications was a result of a lower BET surface area without changing MgO crystal size that determines the theoretical surface area. Increasing MgO crystal size after triple chemical densification led to decrease of the Ψ value. Physical densification yielded $\Psi = 1.7$.

The surface basicity was followed by indicator titration of basic sites, by CO_2-TPD and by FTIR of adsorbed CO_2. The specific surface basicity of the MgO material was measured by titration of benzoic acid with phenolphthalein as the indicator ($pK_a > 9$) as presented in Table 1. Although that method [19] was developed for MgO with a lower surface area of 16 $m^2\,g^{-1}$, its application for higher surface

Table 1
Surface basicity of nanocrystalline MgO materials calcined at 823 K.

MgO material preparation	B [mmol g^{-1}]	B [mmol m^{-2}] × 10^3
Calcination of starting Mg-aerogel	1.2	5
Calcination of Mg-aerogel after one chemical densification	1.5	7
Calcination of Mg-aerogel after two chemical densifications	3.9	40
Calcination of Mg-aerogel after three chemical densifications	2.6	30
Calcination of Mg-aerogel after cold press treatment (physical densification)	1.9	11

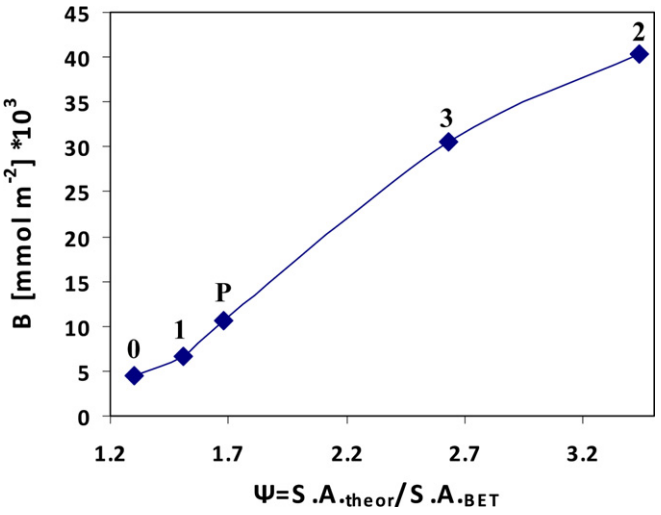

Fig. 4. Correlation between the aggregation ratio of nanocrystals in MgO materials and their surface basicity. The index next to points refers to number of chemical densifications; P — physical densification.

area MgO materials in this study is viable. After two chemical densifications the basicity per gram MgO increased by a factor of 3.2, while the specific basicity per 1 m^2 — by an order of magnitude (Table 1).

The specific basicity shown in Fig. 4 increased almost proportionally with the aggregation ratio of the MgO nanocrystals, independent of the densification strategy. The Hammett indicators are nonselective to the acid/base type [20,21]. Phenolphthalein as an acid indicator is able to protonate both Lewis and Brønsted basic sites thus representing the total concentration of sites with the basic strength sufficient to transform the indicator to its conjugated base form ($pK_a > 9$). The effect of MgO densification on relative concentrations of different surface basic sites (Lewis and Brønsted) was investigated by FTIR of adsorbed CO_2 molecules. The information about the effect of MgO densification on the relative distribution of surface basic sites according to their basic strength was collected using CO_2-TPD.

FTIR spectra of CO_2 adsorbed on the starting Mg-aerogel and double chemically densified aerogel both calcined at 823 K, were recorded over the range of 1100–1900 cm^{-1} (Fig. 5). The detected bands are ascribed to asymmetric and symmetric O–C–O stretching and C–OH bending modes in three types of surface species of adsorbed CO_2 [22,23]: unidentate (1360–1400; 1510–1560 cm^{-1}) and bidentate (1320–1340; 1610–1630 cm^{-1}), carbonates on surface basic oxygen ions—Lewis basic sites, and bicarbonate (1220; 1480; 1650 cm^{-1}) linked to surface hydroxyl groups — Brønsted sites. It indicates two types of surface basic sites in both densified (Fig. 5b) and not densified (Fig. 5a) MgO materials. The integral intensity of all bands related to vibrations of adsorbed CO_2 became

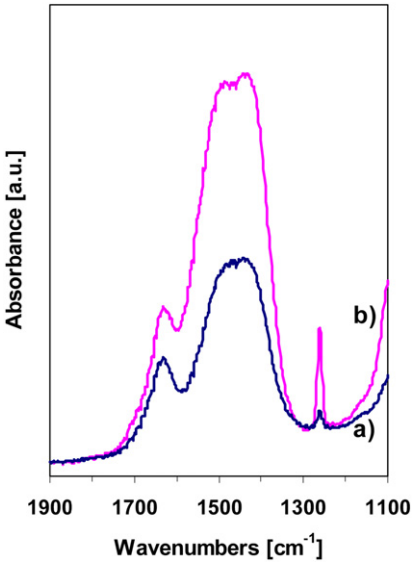

Fig. 5. Infrared spectra of CO_2 adsorbed on MgO materials obtained after calcination at 823 K of: (a) starting Mg-aerogel; (b) Mg-aerogel after double chemical densification.

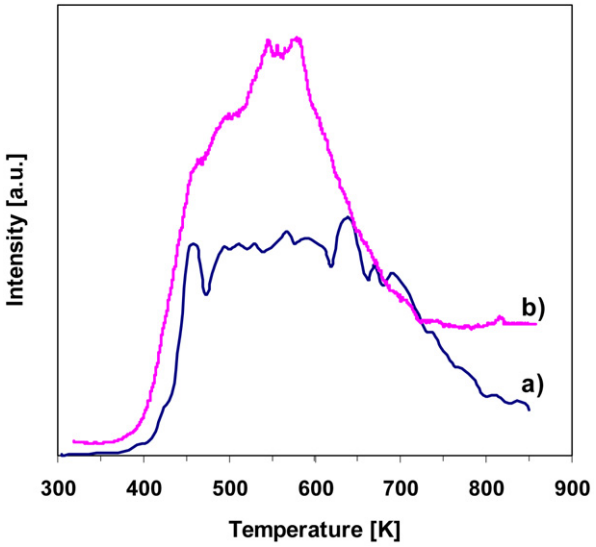

Fig. 6. CO_2-TPD profiles recorded with MgO materials obtained after calcination at 823 K of: (a) starting Mg-aerogel; (b) Mg-aerogel after double chemical densification.

substantially higher after double chemical densification. It shows increasing surface concentrations of both Lewis and Brønsted basic sites, consistent with the results of indicator titration. A significant increase of the integral intensities of bands at 1220 (28.3), 1300–1600 (2.6) and 1600–1750 (2.1) of double chemical densified material was recorded. This means that the amount of Brønsted basic sites (single band centered at 1220 cm^{-1}) increased more than the amount of Lewis sites.

The CO_2-TPD spectra recorded at 300–850 K with MgO materials obtained by decomposition of the starting and doubly chemically densified Mg hydroxide precursor are shown in Fig. 6. At higher temperatures, a significant sintering of MgO nanocrystals strongly decreases the surface area. At the temperatures 400–700 K corresponding to basic sites of average strength in MgO [24], the spectrum of the material obtained by calcination of starting Mg-aerogel represented a set of poorly resolved peaks with about equal intensity (Fig. 6a). Similar spectra were recorded with commercial MgO materials hydrated [25] or as-obtained [24,26]. At

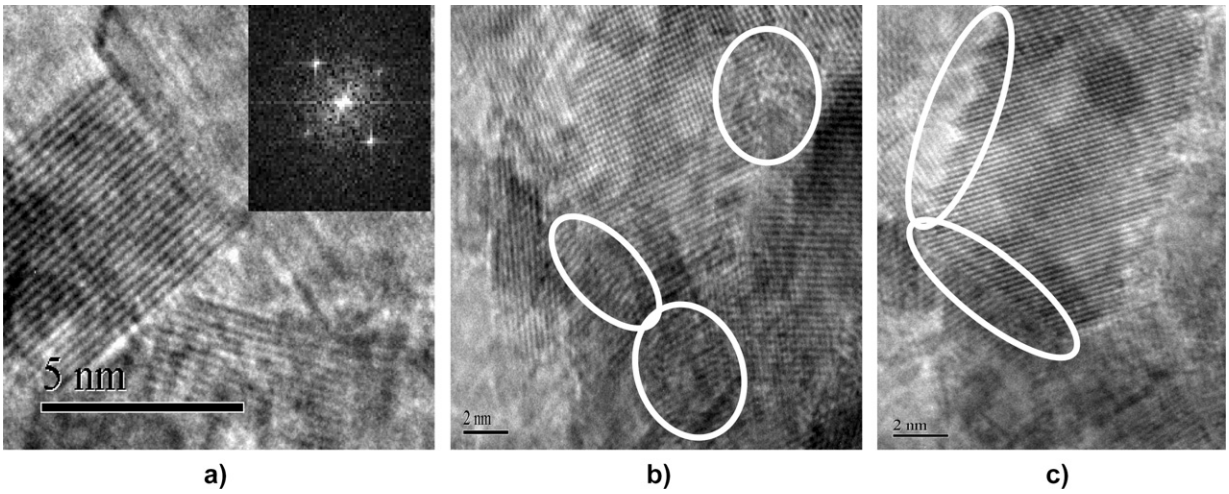

Fig. 7. HRTEM micrographs of MgO materials calcined at 823 K: (a) starting Mg-aerogel; (b, c) Mg-aerogel after two chemical densifications. The areas of crystallographic disorder and saw-edged GBs are indicated with white circle.

higher temperatures >700 K corresponding to strong basic sites in MgO [24] the intensity of TPD peak recorded with this sample gradually decreased as observed in [27,28] for materials obtained by hydration–dehydration of commercial MgO. Double chemical densification of the Mg-aerogel precursor caused a strong increase of the intensity of TPD signal recorded with calcined MgO both in low- and high-temperature ranges (Fig. 6b). The constant value of the CO_2 signal in the 723–873 K range for the doubly densified sample and the fact that its value measured with the not densified MgO markedly decreased indicate a significantly higher concentration of stronger basic sites in the densified material, consistent with indicator titration and FTIR data. It means that double chemical densification of Mg-aerogel precursor caused proportional increase of the concentration of basic sites of average and high basic strength in the calcined MgO material.

Increasing of the MgO crystal aggregation ratio Ψ without a significant increase of crystal size — caused by densification of the Mg hydroxide precursor — is a consequence of higher contact interface between the MgO nanocrystals, as predicted above. Actually, it is caused by blocking access to the crystal surface at the contact interface, making it unavailable for N_2-adsorption. This strongly decreases the measured surface area with its theoretical value calculated on the basis of MgO crystal size almost unchanged. The increase of aggregation ratio Ψ reflects densification of the nanocrystalline MgO material. It is consistent with the more then two-fold reduction of the pore volume in MgO nanocrystals aggregates from 1.33 to 0.60 $cm^3\,g^{-1}$ in MgO after two chemical densifications of the Mg-aerogel precursor. The established correlation between the surface basicity and MgO crystal aggregation ratio (Fig. 4) indicates the creation of additional basic sites in the nanocrystals contact interface areas. The development of GB and LCSI in the nanocrystals contact interface as a result of densification of nanocrystalline MgO material was confirmed by comparative materials characterization using HRTEM, XRD and XPS techniques.

3.2. Formation of novel grain boundaries and LCSI as a result of MgO densification

The formation of GB was examined in HRTEM micrographs. Fig. 7a shows isolated MgO nanocrystals with straight (plane) edges formed after calcination of the starting Mg-aerogel at 823 K. The inset in Fig. 7a shows Fourier transform of the high resolution lattice image of MgO nanocrystals in this material. The measured interplane distance of 2.1 Å corresponds to the direction (200) in cubic periclase structure of MgO crystals. Densification of the precursor led to formation of MgO nanocrystal aggregates with displacement of atoms, shifts of atomic planes and forms saw-edged GB at nanocrystal joining areas, as can be seen in Figs. 7b and 7c. The creation of areas with atomic disorder due to mutual penetration of surface ions into the bulk of neighbor MgO nanocrystals by diffusion in opposite directions implies that more distorted zones were formed (Figs. 7b and 7c).

The formation of LCSIs upon densification of the MgO precursor was detected by XPS, confirming an alteration of the electronic state of the surface ions as a result of changing their coordination in distorted GB areas. The XPS spectra recorded for O1s, Mg2p and C1s core levels are shown in Fig. 8. The binding energies (BE) matching the components of these spectra obtained after deconvolution of corresponding envelopes and their relative contributions are given in Table 2. Deconvolution of the O1s core envelope in XPS spectra of MgO obtained by calcination of the starting Mg-aerogel yielded two components characteristic for lattice oxygen (BE 530.9 eV) and surface carbonate species (BE 532.8 eV) [23,29,30] that comprise 81 and 19% of the total envelope area (Fig. 8a-1). The double chemical densification (Fig. 8a-2) shifted the BE corresponding to lattice oxygen in the calcined MgO to 530.3 eV, caused an increase of the contribution of the component characteristic for surface carbonate species to 26% and appearance of a novel component centered at BE of 531.7 eV that represents the surface hydroxyl groups [23]. The shift of the BE of lattice oxygen to lower value could be interpreted as an increase of the effective negative charge on the surface oxygen ions, reflecting, in turn, the increase of basic strength of oxygen atoms due to prevailing of their ionic state with enhanced electron density [31]. This is a result of increasing the share of surface oxygens with low coordination at distorted GB areas appeared after densification. It is consistent with the detected growth by a factor of 1.5 of the relative amount of surface carbonates. This reflects an increase of the concentration of surface basic sites able to adsorb CO_2 from the ambient in agreement with CO_2-TPD data. Appearance of additional peak corresponding to surface hydroxyls after chemical densification of Mg-aerogel is unswerving to the FTIR data detected an increase of the amount of Brønsted basic sites.

The coexistence of lattice Mg-ions with Mg-ions associated with hydroxyl groups and carbonate species at the surface of MgO generally yields an envelope of Mg2p core consisting of three components with BE increasing from 49.3–50.2 to 50.4–50.8 and then 50.9–51.7 eV, respectively [23,29,30,32–34]. Similar three component XPS spectra were recorded with calcined Mg-aerogels

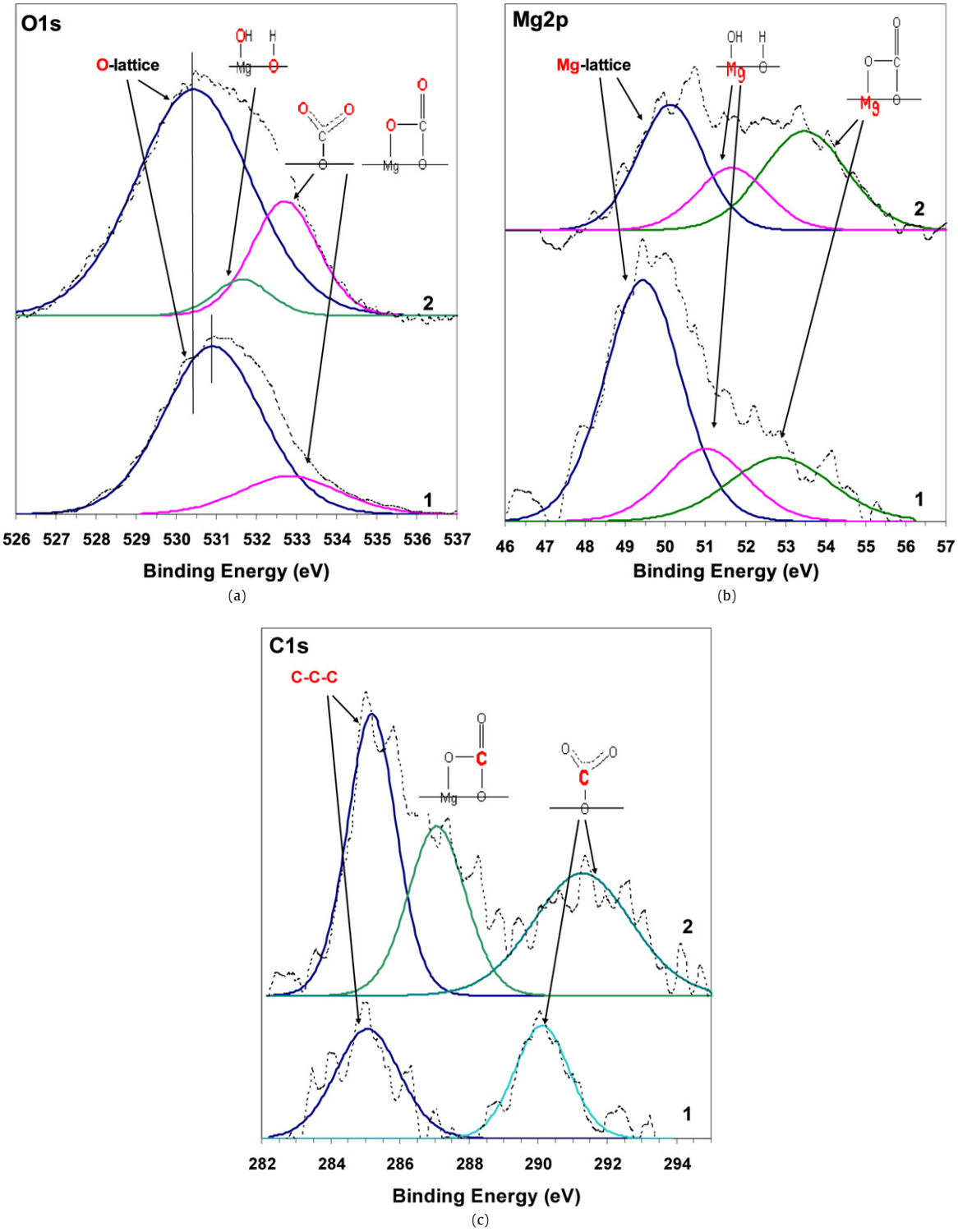

Fig. 8. XPS spectra recorded at the O1s (a), Mg2p (b) and C1s (c) cores of surface atoms in MgO materials calcined at 823 K: 1 — starting Mg-aerogel; 2 — Mg-aerogel after two chemical densifications.

(Fig. 8b). The double chemical densification shifted the BE corresponding to lattice magnesium in the calcined MgO from 49.7 eV in not densified material (Fig. 8b-1) to 50.2 eV (Fig. 8b-2, Table 2). It also caused a significant increase of the contribution of the two components characteristic for adsorbed Mg–O–COO moieties and surface Mg-hydroxyl species from 14 to 32 and from 11 to 25%, respectively (Table 2). The shift of BE of lattice Mg-ions reflects the prevailing of their ionic state with decreased electrons density in agreement with the prevailing of surface oxygen ionic state with enhanced electron density in densified MgO material. It could be interpreted as a result of increasing the share of surface magnesium ions with low coordination at distorted GB areas appeared after densification. The increase of contribution of components related to Mg-ions bonded to surface carbonate and hydroxyl groups reflects a strong increase of CO_2 adsorption at the surface of MgO obtained from densified precursor. It is consistent with the CO_2-TPD and XPS spectra of the O1s (Fig. 8a) and C1s core level (Fig. 8c). This allows inferring a relative increase of the con-

Table 2
Binding energy values and contributions of spectra components obtained for the nanocrystalline MgO calcined at 823 K.

MgO material preparation	O1s (eV)	At%	Mg2p (eV)	At%	C1s (eV)	At%
Calcination of starting Mg-aerogel	530.9	82	49.7	75	285.0	61
	532.9	18	51.0	11	289.8	39
			52.8	14		
Calcination of Mg-aerogel after two chemical densifications	530.3	69	50.2	43	285.0	40
	531.6	5	51.7	25	289.1	28
	532.7	26	53.5	32	292.4	32

centration of surface Mg-ions involved in formation of Lewis and Brønsted basic sites.

In case of electrons belonging to the C1s core the envelope of XPS spectra besides a component related to adventitious carbon (BE 285.0 eV), contained one or two additional components which contribution to the total spectra increased from 39 to 60% after densification of MgO precursor (Fig. 8c, Table 2). These components with BE 289.8 eV (MgO obtained by calcination of the starting Mg-aerogel, Fig. 8c-1) and with BE 287.3 and 291.5 eV (MgO obtained by calcination of Mg-aerogel after double chemical densification, Fig. 8c-2) are related to adsorbed carbonate species [30,32,35]. The peak corresponding to lower BE of C1s electrons could be attributed to bidentate carbonate associated with Mg-cations [35] while the second contribution — to unidentate surface carbonate species. The detected increase of contribution of peaks corresponded to uni- and bidentate surface carbonates to XPS spectra can be interpreted as an increase of surface concentration of both Lewis and Brønsted basic sites in agreement with CO_2-TPD and FTIR data (Section 3.1). As was concluded above, this is a result of increasing the share of Mg- and O-ions with low coordination appeared at distorted GB areas after densification of magnesia material.

The appearance of a wide reflection (amorphous halo) in XRD patterns centered at $2\theta = 36^\circ$ could also serve as evidence for the irregular arrangement of ions in the GB areas formed in the densified MgO materials (Figs. 1c and 1d). No peaks corresponding to either $Mg(OH)_2$ or to crystalline MgO phase with cubic structure were found at this diffractogram area. The detected reflection corresponds to an amorphous MgO phase with a short range order at the distance of 2.5 Å that reflects the interatomic distances in disordered MgO_x building units. The relative amount of this amorphous MgO phase estimated from XRD data increased from zero in MgO obtained by calcination of the starting aerogel to 20% after two chemical densifications and to 7% after physical densification. The HRTEM analysis of the MgO material obtained from doubly densified hydroxide precursor detected no particles with a shape different significantly from that of cubic MgO nanocrystals. Parallel fringes characteristic of atomic layers in the periclase structure were displayed in the images of all nanoparticles. These findings consent to attribute the amorphous phase detected by XRD at least partially to the atomic disorder in the GB areas. Changes in the fraction of amorphous phase correlated well with the increase of surface basicity.

3.3. Catalytic activity in base-catalyzed reactions of densified nanocrystalline MgO

The catalytic performance of the calcined precursor aerogel, in terms of reaction rates, was compared with that of the doubly densified material (which had the highest surface basicity) in two organic reactions: in the condensation of benzaldehyde with malononitrile (RI) and in the transesterification of phenylacetate with 1-phenylethanol (RII) (Scheme 2). RI is used for testing the performance of basic catalysts [36–38] that requires the basic sites with

Table 3
Effect of chemical densification of Mg-aerogel on its catalytic activity after calcination at 823 K.

Reaction	Catalytic activity	MgO material preparation	
		Starting Mg-aerogel	Mg-aerogel after two chemical densifications
Condensation of benzaldehyde with malonitrile (RI)	$Rate_w$ [mmol g^{-1} h^{-1}]	360	971
	$Rate_S$ [mmol m^{-2} h^{-1}]	1.4	9.0
	TOF [h^{-1}]	299	248
Transesterification of phenyl acetate with 1-phenylethanol (RII)	$Rate_w$ [mmol g^{-1} h^{-1}] $\times 10^3$	300	4300
	$Rate_S$ [mmol m^{-2} h^{-1}] $\times 10^3$	1	40
	TOF [h^{-1}] $\times 10^3$	270	1100

$pK_a > 11$ [37]. RII was selected for testing higher base strength, since pK_a of phenyl acetate is equal to 14.3 [39]. Transesterification reactions require stronger basic sites than Knoevenagel condensation and proceed at much slower rate [40]. The complete selectivity to benzylidene malononitrile (RI) and α-methylbenzylacetate (RII)) correlates the measured reaction rates directly to concentrations of basic sites on the surface of MgO materials.

The reaction rate (based on catalyst mass) of MgO obtained by calcination of doubly densified Mg-aerogel precursor was 2.7 and 14.3 times higher than MgO obtained from the starting aerogel, for the first and second reactions, respectively (Table 3). The values for the TOF for the first reaction were about the same before and after precursor densification, while for the second reaction the TOF increased by a factor of about 4 for the MgO obtained from the doubly densified aerogel. This difference can be explained in terms of the demand in the second reaction for stronger or protonic basic sites, whose share in the measured total basicity increased after double densification of the MgO precursor. The greatest differences in catalytic activity were found when the activity was normalized per unit of catalyst surface. They represent the quantitative difference between the performance of MgO surfaces in starting and densified materials. Densification that forms GB areas with atomic disorder increases by about an order of magnitude (Table 1) the surface concentration of LCSI generating the surface basic sites. This is directly reflected by the difference of specific catalytic performance in both testing reactions (Table 3).

The stability of doubly densified MgO material was tested in reaction RI. A run was conducted at standard conditions to reach 74% conversion after 2 h. The two reactants were added to reach the same initial concentrations. The interim conversions in the second run were very similar to those in the first, reaching 73% conversion after 2 h.

4. Conclusions

The nanostructured MgO material obtained from densified magnesium hydroxide aerogel precursor revealed higher surface chemical reactivity as a base solid catalyst, possessing higher amount of basic surface active sites, compared with MgO obtained from the parent undensified magnesium aerogel. This is a result of creation of atomic disorder formed at the interface of crystal grains (grain boundaries) between MgO nanocrystals. Densification of aerogel precursor increases the MgO nanocrystals aggregation ratio that favors formation of grain boundaries as a source of the surface basic chemical functionality.

The presented data thus illustrate that designing high-angle or coincidence GB in nanocrystalline ionic crystals such as MgO constitutes an effective and viable tool for increasing its catalytic activity.

Acknowledgments

This study was supported by the Israeli Science Foundation (Grant No. 739/06) and the Blechner Foundation. The authors gratefully acknowledge the help of Dr. D. Mogylyansky and Dr. A. Erenburg in conducting the XRD characterizations.

References

[1] R.A. Van Santen, M. Neurock, in: Molecular Heterogeneous Catalysis: Conceptual and Computational Approach, Wiley–VCH, Weinheim, 2006, Chap. 5.
[2] M.I. Molotskii, Kinet. Katal. 15 (1974) 758.
[3] J. Nowotny, NATO ASI Ser. Ser. E 173 (1989) 205.
[4] D.M. Saylor, A. Morawiec, G.S. Rohrer, Acta Mater. 51 (2003) 3675.
[5] D.M. Saylor, A. Morawiec, G.S. Rohrer, Acta Mater. 51 (2003) 3663.
[6] M. El-Hofy, Defect Diffus. Forum 251–252 (2006) 13.
[7] Y. Pang, P. Wynblatt, J. Am. Ceram. Soc. 88 (2005) 2286.
[8] Y. Sato, T. Yamamoto, Y. Ikuhara, J. Am. Ceram. Soc. 90 (2007) 337.
[9] S. Royer, D. Duprez, S. Kaliaguine, Catal. Today 112 (2006) 99.
[10] M. Che, A.J. Tench, Adv. Catal. 31 (1982) 77.
[11] H. Hattori, Appl. Catal. A 222 (2001) 247.
[12] C. Chizallet, G. Costentin, H. Lauron-Pernot, J.M. Krafft, P. Bazin, J. Saussey, F. Delbecq, P. Sautet, M. Che, Oil Gas Sci. Technol. 61 (2006) 479.
[13] A.P. Alivisatos, J. Phys. Chem. 100 (1996) 13226.
[14] R. Narayanan, C. Tabor, M.A. El-Sayed, Top. Catal. 48 (2008) 60.
[15] K.C. Mundim, V. Liubich, S. Dorfman, J. Felsteiner, D. Fuks, G. Borstel, Solid State Commun. 118 (2001) 301.
[16] T. Hammerschmidt, A. Kersch, P. Vogl, Phys. Rev. B 71 (2005) 205409/1.
[17] S. Utamapanya, K.J. Klabunde, J.R. Schlup, Chem. Mater. 3 (1991) 175.
[18] S.J. Gregg, K.S.W. Sing, Adsorption, Surface Area and Porosity, 2nd ed., Academic Press, London, 1982, 303 pp.
[19] P. Kaessner, M. Baerns, Appl. Catal. A 139 (1996) 107.
[20] H.G. Karge, in: G. Ertl, H. Knozinger, F. Schuth, J. Weitkamp (Eds.), Handbook of Heterogeneous Catalysis, Wiley–VCH, Weinheim, 2008, p. 1096.
[21] K. Hashimoto, T. Masuda, H. Sasaki, Ind. Eng. Chem. Res. 27 (1988) 1792.
[22] J.I. Di Cosimo, V.K. Diez, M. Xu, E. Iglesia, C.R. Apesteguia, J. Catal. 178 (1998) 499.
[23] F. Khairallah, A. Glisenti, J. Mol. Catal. A Chem. 274 (2007) 137.
[24] Z. Liu, J.A. Cortes-Concepcion, M. Mustian, M.D. Amiridis, Appl. Catal. A 302 (2006) 232.
[25] A.S. Ndou, N. Plint, N.J. Coville, Appl. Catal. A 251 (2003) 337.
[26] J.H. Zhu, Y. Wang, Y. Chun, Z. Xing, Q.H. Xu, Mater. Lett. 35 (1998) 177.
[27] G. Zhang, H. Hattori, K. Tanabe, Appl. Catal. 36 (1988) 189.
[28] E.J. Doskocil, S.V. Bordawekar, R.J. Davis, J. Catal. 169 (1997) 327.
[29] H.B. Yao, Y. Li, A.T.S. Wee, Appl. Surf. Sci. 158 (2000) 112.
[30] F. Khairallah, A. Glisenti, Surf. Sci. Spectra 13 (2006) 58.
[31] Y. Okamoto, M. Ogava, A. Maezawa, T. Imanaka, J. Catal. 112 (1988) 427.
[32] D.K. Aswal, K.P. Muthe, S. Tawde, S. Chodhury, N. Bagkar, A. Singh, S.K. Gupta, J.V. Yakhmi, J. Cryst. Growth 236 (2002) 661.
[33] D.K. Aswal, K.P. Muthe, A. Singh, S. Sen, R. Shah, L.C. Gupta, S.K. Gupta, V.C. Sahni, Physica C 363 (2001) 208.
[34] S. Ardizzone, C.L. Bianchi, M. Fadoni, B. Vercelli, Appl. Surf. Sci. 119 (1997) 253.
[35] R. Mariscal, J. Soria, M.A. Pena, J.L.G. Fierro, J. Catal. 147 (1994) 535.
[36] Y. Xia, R. Mokaya, Angew. Chem. Int. Ed. 42 (2003) 2639.
[37] M.J. Climent, A. Corma, V. Fornes, A. Frau, R. Guil-Lopez, S. Iborra, J. Primo, J. Catal. 163 (1996) 392.
[38] M.J. Climent, A. Corma, S. Iborra, A. Velty, J. Mol. Catal. A Chem. 182–183 (2002) 327.
[39] A.A. Neverov, N.E. Sunderland, R.S. Brown, Org. Biomol. Chem. 3 (2005) 65.
[40] A. Corma, S. Iborra, S. Miquel, J. Primo, J. Catal. 173 (1998) 315.